ZIBELINE INTERNATIONAL™ PUBLISHING

ISSN: 2616-4302 (Online)
CODEN: AMMCFL

Acta Mechanica Malaysia (AMM)

DOI: http://doi.org/10.26480/amm.02.2023.114.121

RESEARCH ARTICLE

FLUID DYNAMIC PERFORMANCE AND PERFORMANCE ANALYSIS OF A NOVEL FLEXIBLE OSCILLATING WIND TURBINE

Dayu Zhang*

School of Energy and Power Engineering, Xi'an Jiaotong University, Xi'an, P.R. China
**Corresponding author Email address: 15734010074@163.com*

ARTICLE DETAILS

Article History:

Received 10 June 2023
Revised 14 July 2023
Accepted 18 August 2023
Available online 22 August 2023

ABSTRACT

While the variable pitch angle design has been proven to significantly enhance the performance of vertical axis wind turbines, its implementation requires the addition of extra mechanical devices, such as a chain-and-sprocket system. These additional mechanisms not only increase system friction and produce extra vibrations but also cause vertical axis wind turbines to lose their omnidirectional characteristics. To address this issue, this study proposed a novel flexible oscillating wind turbine, wherein the function of changing the pitch angle is accomplished through the deformation of flexible blades. To reveal the internal flow field mechanism of this novel turbine, particle image velocimetry experiments were conducted. The results indicate that the flexible blade can alter its posture to form a suitable angle of attack under different azimuth angles. In the downstream region, the blades spread out to generate a substantial positive torque. In contrast, in the upstream region, the blades are in a diversion state, always maintaining a small angle of attack to avoid generating excessive negative torque. Wind tunnel experiments were carried out on the flexible oscillating wind turbine to explore the effects of wind speed and key geometric parameters on the turbine's performance. The results show that the novel flexible oscillating wind Turbine maintains high efficiency even under low wind speed conditions.

KEYWORDS

Vertical axis wind turbine; variable pitch angle; wind tunnel experiment

1. INTRODUCTION

The Earth's atmosphere harbors immense kinetic energy, with the global wind energy reserve estimated at approximately 1.3 trillion kilowatts, of which 200 billion kilowatts are considered exploitable. Wind energy, as one of the fastest-growing renewable energy sources globally, is seeing a continuous increase in total installed capacity due to its sustainability, abundance, and relatively low environmental impact. In 2022, 78 GW of wind energy capacity was added, boosting the total installed wind energy capacity to 906 GW (GWEC, 2022). Among the wind turbines that significantly contribute to the global renewable energy, Horizontal Axis Wind Turbines (HAWTs) currently dominate, holding a substantial market share (Islam et al., 2013). The technological maturity and high efficiency of HAWTs make them the preferred choice for large-scale wind energy conversion systems (Sahu, 2018).

However, in small-scale distributed wind energy conversion systems, the application of Vertical Axis Wind Turbines (VAWTs) is garnering increasing attention (Tummala et al., 2016). Due to VAWTs are omnidirectional, they can capture wind energy from all directions without any yaw device and enhance their efficiency in turbulent flow regions. Additionally, VAWTs demonstrate superior structural strength, enabling them to withstand typhoon-level winds without requiring pitch-regulated devices. Small-scale distributed wind energy conversion systems are hard-pressed to accommodate excessive auxiliary starting devices, such as auxiliary motors and pitch change devices. In the absence of these auxiliary devices, VAWTs feature low cut-in wind speeds, widening their range of application. Therefore, small VAWTs are extensively utilized in distributed meteorological stations and lampposts on remote highways (Akwa et al., 2012).

However, VAWTs have a pressing shortcoming to address: their relatively low power coefficient (Miliket et al., 2022; Tian et al., 2014). The low efficiency of VAWTs is due to their time-varying attack angle during operation, resulting in negative torque being produced at more than 50% of the azimuthal angle. When the rotor operates at low rotational speeds, the proportion of negative torque increases even further. For HAWTs, blade's attack angle is fixed at all azimuthal angles at a certain rotational speed, allowing for the adjustment of various blade parameters to maximize torque. However, the situation is different for VAWTs. For VAWTs, the attack angle and force arm of the blades are constantly changing. As such, there isn't an appropriate pitch angle that allows the blades to generate maximum torque at any azimuthal angle (Rezaeiha et al., 2017). Some researchers conducted simulation studies on lift-type VAWTs with different pitch angles (Guo et al., 2019). Their results found that a larger pitch angle can produce greater positive torque in the upstream region, but it also increases the range and peak of negative torque produced in the downstream region. Conversely, a smaller pitch angle can generate greater positive torque in the downstream region, but it reduces the peak positive torque in the upstream region.

To allow the blades to have an appropriate angle of attack at different azimuth angle and thereby increase the power coefficient of the wind turbine, a group researchers proposed a novel VAWT that uses a linkage device to change the pitch angle (Elkhoury et al., 2015). Depending on the different azimuth angle, this design alters the blade pitch angle to achieve the appropriate angle of attack. In the same experimental environment, the VAWT with variable pitch angle demonstrated nearly 30% improved

Quick Response Code	Access this article online	
	Website: www.actamechanicamalaysia.com	DOI: 10.26480/amm.02.2023.114.121

Cite the Article: Dayu Zhang (2023). Fluid Dynamic Performance and Performance Analysis of a Novel Flexible Oscillating Wind Turbine. *Acta Mechanica Malaysia, 6(2): 114-121.*

coefficient compared to fixed pitch angle VAWT, along with better startup performance. Some researchers also designed a VAWT with variable pitch angle using a spring-slider device and achieved greater self-starting ability and efficiency (Douak et al., 2018). Similar variable pitch angle designs can be applied to drag-type VAWTs operating at low *TSR*. ElCheikh et al. designed a chain-and-sprocket device, allowing the blades to oscillate over a wider range (ElCheikh et al., 2018). Wind tunnel tests revealed that this drag-type VAWT with variable pitch angle could achieve a power coefficient of over 0.2 at 10 m/s wind speed.

However, although variable pitch angle devices can enhance the performance of VAWTs, there are not any practical application. This is because such a VAWT would add extra mechanical structures and cause losing its omnidirectional characteristics. Using variable pitch angle devices would necessitate adding a yaw devise, such as a tail rudder, which would not only reduce the efficiency but also the reliability of the wind turbine. Furthermore, the energy needed to change the pitch angle and the friction created in the process must be supplied by the wind turbine itself. As the system runs over time, its energy loss would become more significant, and due to the rigidity of the blades, changing their position could generate extra vibrations.

To address this issue, this paper proposes a novel flexible oscillating wind turbine. The function of changing the pitch angle is accomplished by the deformation of flexible blades. Figure 1 illustrates the concept of this innovative VAWT. This wind turbine is comprised of upper and lower end plates, and centrally symmetrically mounted flexible oscillating blades (Figure 2). The blades consist of rectangular blade frames and rectangular flexible membrane blades. One side of the flexible membrane blades remains unattached to the blade frame, allowing them to deform in response to the incoming flow. The flexible membrane blades can be attached using small sail eyelet connections, socket connections, or mixed eye-and-socket connections. Materials such as carbon fiber cloth, canvas, or high-polymer plastic film can be selected for the flexible membrane, depending on the wind field strength in the region (Fang et al., 2022).

Due to the flexible membrane blades deforming under the action of the incoming flow, and thus changing their pitch angle at different azimuth angle, the flexible oscillating wind turbine can obtain positive torque over a more extensive azimuth angle range compared to other vertical-axis hydrokinetic turbines with fixed blades. Compared to VAWTs that rely on rigid mechanical devices to change pitch angle, the flexible oscillating VAWT described in this paper can alter the pitch angle without any additional mechanical structures, retaining its omnidirectional characteristics. Moreover, the inertia of the flexible membrane blades is extremely low, resulting in reduced energy loss and vibrations caused by changing the pitch angle.

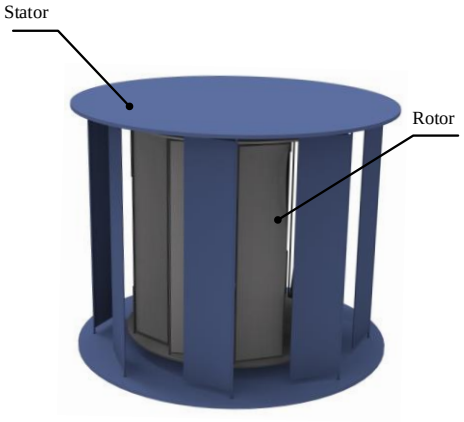

Figure 1: Schematic of Flexible Oscillating Wind Turbine With Deflector Synthesis Of Cus Nanoparticles And Study Of Its Photocatalytic Activity

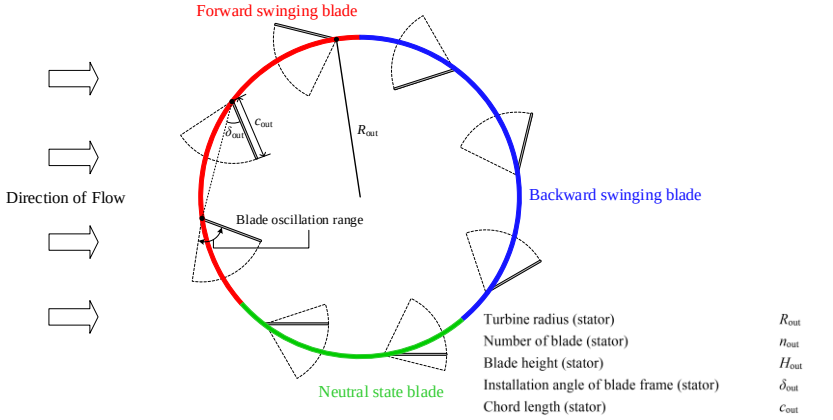

(a) Working principle diagram of deflector

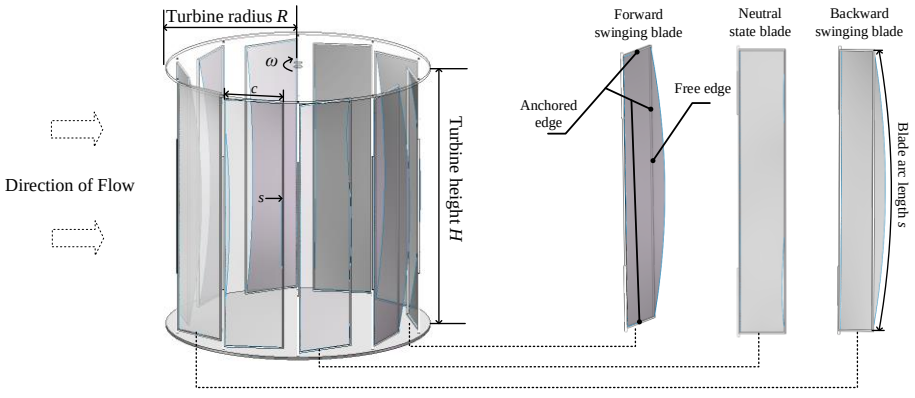

(b) Structure diagram of rotor

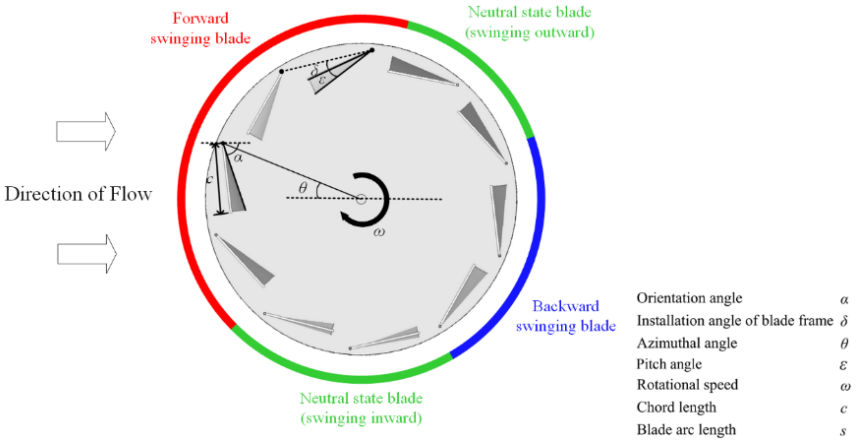

(c) Working principle diagram of rotor

Figure 2: Structure and operational schematic of flexible oscillating wind turbine with deflector

In addition, a wind deflector for flexible oscillating wind turbines was designed to further enhance its performance while ensuring the omnidirectionality of the VAWT. Wind tunnel experiments were conducted on this flexible oscillating wind turbine with deflector to explore the effects of wind speed and key geometric parameters on the performance of the wind turbine. Additionally, to reveal the internal flow field mechanism of the novel wind turbine, this paper conducts Particle Image Velocimetry (PIV) experiments on it using the principle of similarity.

2. Working Principle

The flexible membrane blades alter their posture, i.e., vary pitch angle to swing outward or inward, based on different azimuthal angle θ (Figure 3). In the inflow region (-45° < θ < 45°), the blades swing inward, indicating a negative pitch angle, to achieve smaller and gradually increasing angles of attack. This posture allows the blades to generate a significant upward lift. In this region, the upward lift has a larger moment arm, thereby producing a counterclockwise positive torque.

When the blades rotate into the downstream region (45° < θ < 135°), the drag has a larger lever arm, necessitating the blades to align with the incoming flow at a large angle of attack in order to generate a large positive torque. Thus, the blades in this region first swing inward to the critical point where the frame is parallel to the incoming flow, and then quickly transition to swing outward to achieve the large angle of attack. As the blades rotate to the outflow region (135° < θ < 225°), the downward lift has a larger lever arm. Therefore, in this area, as much downward lift as possible is required, so the optimal attack angle for the blades in this region lies within the 90°-180° range. In this area, the blades swing outward, ensuring that the attack angle of the blades is within an appropriate range.

When the blades rotate to the upstream region (225° < θ < 315°), the lever arm of the drag is large, and the relative speed of the blades in this region is high. Therefore, even a small angle of attack can generate large drag. Reducing the negative torque generated in this region is key to improving the overall efficiency of the wind turbine. In this region, the anchored edge of the blade is close to the direction of the incoming flow, with the free edge of the blade trailing behind the anchored edge. Therefore, the blades in this region maintain a diversion state. As the blade rotates, the posture of the blade gradually transitions from an outward swing to an inward swing, always maintaining an alignment nearly parallel to the direction of the flow.

Due to the structural characteristics of the flexible membrane blade, the change in pitch angle is largest at the center of the turbine axis and smallest at the edge of the turbine. The amount of change in the pitch angle depends on the blade arc ratio (s/H) and the material properties of the flexible membrane.

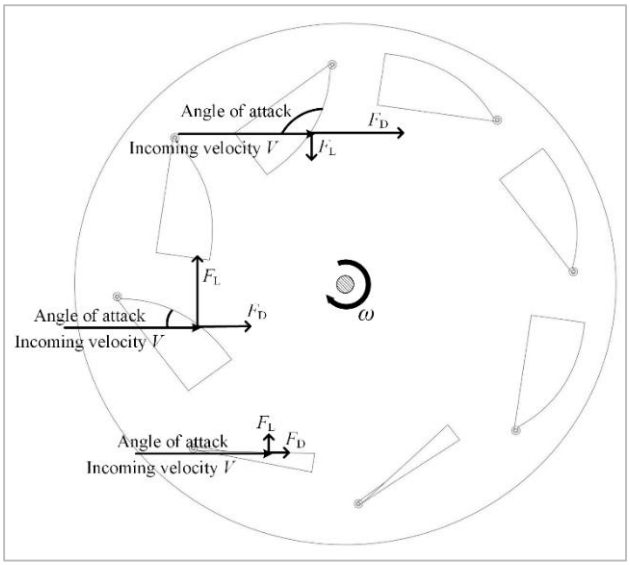

Figure 3: Operational principle of the novel flexible oscillating wind turbine

The deflector designed in this paper is composed of rectangular rigid blades installed symmetrically around the center, which can swing within a certain sector area. Compared to adding ducting of rotors, curtains, or concentrators on the outside of the wind turbine, the deflector designed in this paper allows the vertical axis wind turbine to retain its omnidirectional properties. The flexible oscillating wind turbine performance is estimated in terms of power coefficient C_P, which is defined as the ratio of power produced by a turbine to the available power in the current as follows:

$$C_P = \frac{T\omega}{0.5\rho\pi R^2 V_\infty^3} \quad (1)$$

where T is the torque produced by the turbine (Nm), ω is the turbine rotational speed (rad s^{-1}), ρ is the density (kg m^{-3}), R is the rotor radius (m), and V_∞ is the current speed (m s^{-1}).

The tip speed ratio (*TSR*) is defined by:

$$TSR = \frac{\omega R}{V_\infty} \quad (2)$$

3. Internal Flow Field of the Turbine

3.1 PIV Experiment Facility

To elucidate the operational mechanism of the flexible oscillating wind turbine, PIV experiments were conducted. However, the wind tunnel's side walls in our laboratory do not meet the observational conditions for PIV experiments. Therefore, a circulating water flume with transparent sidewalls was constructed to carry out the PIV experiments (Figure 4). Given that it's essential to ensure flow similarity between the turbine in the water flume experiments and the turbine mentioned in the subsequent wind tunnel experiments, and considering the high solid of the flexible oscillating wind turbine, it is necessary to maintain a similar Reynolds number for both turbines. Therefore, in this section, the incoming flow speed in the water flume experiment is set to be 0.1m/s, ensuring that the Reynolds numbers for both the wind tunnel and water flume experiments fall within the range of 1×10^5 to 5×10^5.

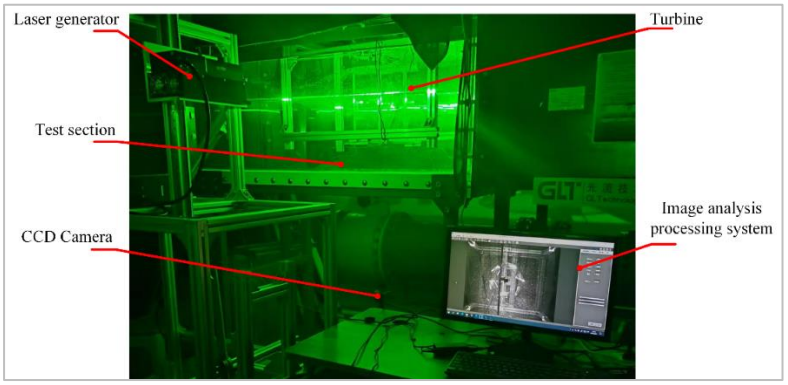

Figure 4: Schematic diagrams of the PIV experiment

The experimental setup, depicted in the schematic diagram of Figure 4, consisted of a circulating water flume with a test section measuring 1000 mm in length, 500 mm in height, and 800 mm in width, including a measurement platform. The walls of the water flume are made of 10 mm thick acrylic, ensuring structural strength while facilitating observation and capturing the internal flow conditions.

The turbine was positioned at the center of the cross-section, with a distance of 500 mm between the upstream entrance and the top of the turbine shaft. The water pump, in combination with a closed-loop control system, allowed for a maximum controllable flow speed of 1 m/s. Simultaneously, PIV experiment was utilized to reveal the internal flow field of the turbine and capture the time-varying state of the flexible oscillating blades. The PIV setup primarily consists of a pulsed laser generator, synchronizer, a charge coupled device (CCD) camera, and image analysis processing system. The pulsed laser generator has a peak power of 10W and can generate a light sheet with a wavelength of 532nm. The CCD camera has a resolution of 2560×2048 pixels and a sampling frequency of 60 Hz. Hollow glass beads with a mean diameter of 50 μm were used as tracer particles. The geometric parameters of the tested turbines are presented in Table 1.

For the flexible membrane blades, the ratio s/H equals 1, meaning the shape of blades is rectangular. The material of the flexible membrane blades is polyethylene, with a tensile modulus of approximately 30 MPa.

3.2 Result of PIV Experiment

Figure 5 demonstrate the internal flow field status of turbines with different n in the PIV experiment under static conditions (TSR= 0) and operating conditions (TSR = 0.4).

Table 1: Geometrical Parameters of Turbines PIV Experiment

Parameter	Symbol	Value
Turbine radius (mm)	R	150
Number of blade	n	6 and 9
Turbine height (mm)	H	300
Installation angle of blade frame (°)	δ	0
Chord length (mm)	c	80
Blade arc length (mm)	s	300

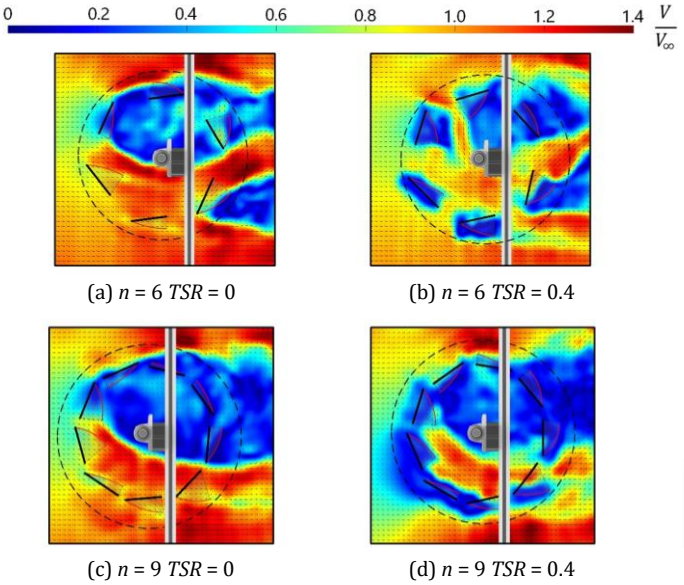

(a) n = 6 TSR = 0 (b) n = 6 TSR = 0.4

(c) n = 9 TSR = 0 (d) n = 9 TSR = 0.4

Figure 5: Flow patterns near the turbine

For the turbine with six blades, the incoming flow through the rotor cavity causes two significant deflections in the inflow region and the outflow region. According to the law of conservation of momentum, blades the inflow and outflow regions receive large positive torques. In the downstream region, the blades try to open as much as possible to generate a large positive torque, whereas the blades in the upstream region remain in the diversion state, always maintaining a small attack angle.

Comparing Figure 5 (a), (b) and (c), (d), it can be observed that an increase in the number of blades significantly enhances the blockage effect of the turbine, reducing the incoming flow speed inside the turbine cavity. Moreover, the increased blockage effect in the outflow region hinders the second deflection of the incoming flow, further affecting power coefficient of the turbine.

The time-varying orientation angle α of turbines with 6 blades and 9 blades is displayed in Figure 6. This paper also derives a model for the torque generated by a flat blade under different azimuth angles and pitch angles, with the incoming flow speed and blade size consistent with the rotor in the PIV experiments. The theoretical model made three simplifying assumptions: First, the blade shape does not change with the incoming flow; second, it ignores the impact of other blades; and third, the lift coefficient and drag coefficient of the flat blade are only related to the attack angle. The lift and drag on the blade are:

$$F_L = \frac{1}{2} C_L \rho V^2 S \tag{3}$$

$$F_D = \frac{1}{2} C_D \rho V^2 S \tag{4}$$

Here, C_L is the lift coefficient and C_D is the drag coefficient of the flat blade , S is the area of the blade. Lift coefficient and drag coefficient of the flat plate blade are given by the following expressions (Jiang et al., 2011) :

$$C_L = \sin 2\alpha \tag{5}$$

$$C_D = 2\sin^2 \alpha \tag{6}$$

The lever arm of the blades in VAWTs varies with the azimuth angle. The expression for the lever arm is:

$$L = (R\cos\theta\,, R\sin\theta) \tag{7}$$

Therefore, the instantaneous torque T obtained by the blade is:

$$T = \frac{1}{2} C_L \rho V^2 SR\cos\theta + \frac{1}{2} C_D \rho V^2 SR\sin\theta \tag{8}$$

Where the relative speed between the blade and the incoming flow also changes with the phase angle and can be expressed as:

$$V = (\omega R\sin\theta - V_\infty, -\omega R\cos\theta) \tag{9}$$

Therefore, the attack angle of the blade can be expressed as:

$$\alpha = \arctan\left(\frac{-\omega\cos\theta R}{\omega\sin\theta R - V_\infty}\right) + (\theta + \delta) \tag{10}$$

By combining equations (8) and (10), the instantaneous torque of the blade can be expressed as:

$$\begin{aligned} Q = {} & \frac{1}{2}\sin 2\left(\arctan\left(\frac{-\omega\cos\theta R}{\omega\sin\theta R - V_\infty}\right) + (\theta + \delta)\right) \rho V_\infty^2 S * \cos\theta R \\ & + \frac{1}{2} 2\sin^2\left(\arctan\left(\frac{-\omega\cos\theta R}{\omega\sin\theta R - V_\infty}\right) + (\theta + \delta)\right) \rho V_\infty^2 S * \sin\theta\, R \end{aligned} \tag{11}$$

Setting the physical quantities to constants consistent with the PIV experiment, the "fsolve" function in MATLAB was used to solve the equation. Afterwards, the torque produced by the blades under different azimuth angles and orientation angles was obtained, and the optimal orientation angle was identified (Figure 6).

Comparing these results with the orientation angle α of the turbine in different azimuth angle, in the azimuthal range of 270 to 90°, the turbine's orientation angle α is close to the optimal value. In the outflow region (azimuth angle of 135-225°), the blades are greatly influenced by the deflection effect of the blades in inflow region, which is significantly different from the single-blade torque model. As shown in Figure 5, the flow speed in this region is relatively low, so an orientation angle α close to 0° and 180° is also quite ideal.

In the outflow region (azimuth angle of 225-315°), where the blades may generate a large amount of drag torque, the turbine's orientation angle α is also close to 0° and 180°. This arrangement helps to avoid the generation of excessive negative torque.

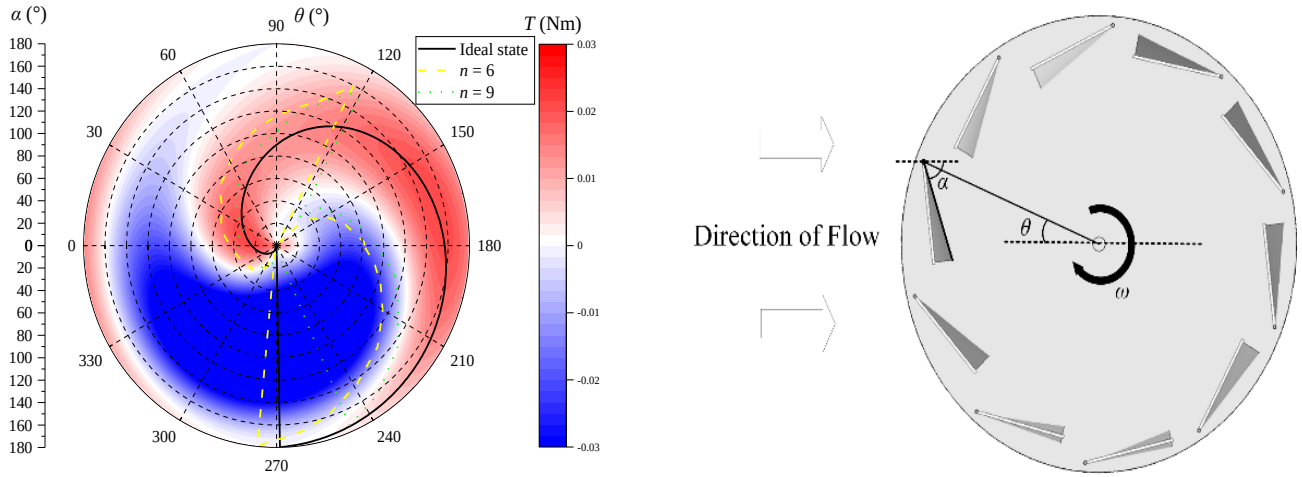

Figure 1: Polar plot of Toque in different azimuth angles and orientation angles

4. Parametric Study

To investigate the effects of the key geometry parameters and wind speed on the performance of the flexible oscillating wind turbine with the deflector, a wind tunnel experiment was conducted and a power measurement platform was built.

4.1 Wind Tunnel Experiment Facility

Figure 7 shows the schematic of the wind tunnel experiment, with a cross-sectional area of 1200mm×1000mm. The geometry parameters of the flexible oscillating wind turbine and the deflector are presented in Figure 7. The material of the flexible membrane blades is ultra-high molecular weight polyethylene fiber, which has a tensile modulus exceeding 2000 Mpa. The deformation caused by external force can be negligible. The blades of the deflector are made of 2mm thick steel plates.

4.2 Blockage Correction Method

The blockage effect imposed by the walls of the wind tunnel can significantly alter the performance of wind turbines relative to that in an unconfined flow. It is essential to adopt a suitable blockage correction method to access an accurate correction factor α.

$$TSR_{\text{correct}} = \frac{TSR_{\text{uncorrect}}}{\alpha} \tag{12}$$

$$C_{\text{p,correct}} = \frac{C_{\text{p,uncorrect}}}{\alpha^3} \tag{13}$$

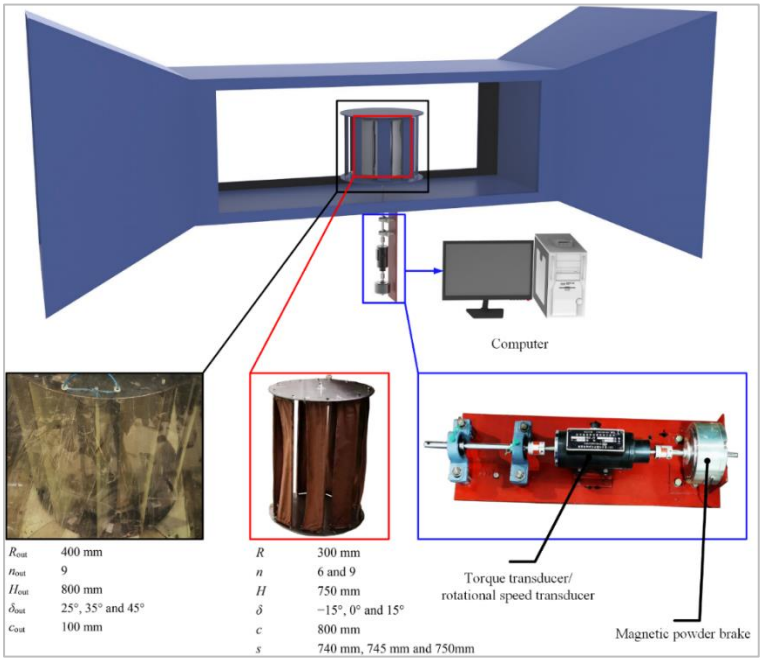

Figure 7: Schematic diagrams of the wind tunnel experiment

Due to the high solidity of the flexible oscillating wind turbine, which falls into the category of drag-type VAWTs, the correction method based on axial momentum actuator disk theory proposed by Glauert results in a nonphysical solution (Glauert, 1935). The rang of the nonphysical solution zone were given in our previous study (Zhang et al., 2023). To solve this issue, Maskell developed a blockage correction method for bluff bodies (Maskell, 1963). Some studies found that Maskell's correction performed better than the actuator disk methods for high-solidity turbines (Kinsey and Dumas, 2017; Ross and Polagye, 2020). In the original bluff body correction, Maskell measured the drag coefficients and base pressures of square flat plates placed perpendicular to the freestream with different blockage ratios. A semi-empirical correction coefficient m was then used to correct the blockage effect. The re-derivation of the expression by is shown as follows (Jeong et al., 2018):

$$m = (C\_Du\ \beta - C\_Pb - \sqrt{((C\_Du\ \beta - C\_Pb\ )\text{^}2 - 4C\_Du\ (1 - C\_Pb\ )\beta)})/2(1 - C\_Pb\ )\beta \quad (14)$$

$$\alpha = \frac{V_\infty'}{V_\infty} = \sqrt{\frac{1}{1-m\beta}} \quad (15)$$

where C_{pb} is the base-pressure coefficient. Jeong extended the Maskell correction method to vertical-axis turbines based on this method. as follows (Jeong et al., 2018):

$$m = \left(1 - \frac{C_{Df}}{C_{Du}}\right)\frac{1}{\beta} \quad (16)$$

The regression curve for the correction coefficient as a function of blockage ratios was calculated and plotted in Figure 8.

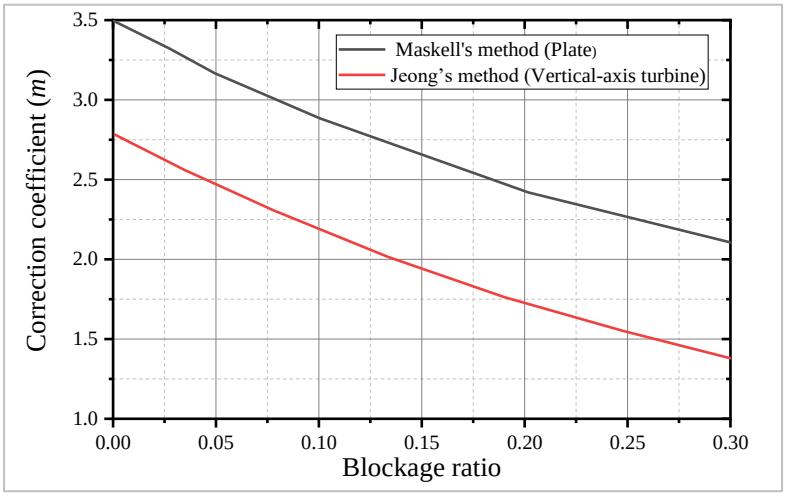

Figure 8: Correction coefficients m in different blockage ratio

Our previous research demonstrated that Jeong's method can correct the blockage effect of vertical axis turbines with a relative error of about 5% (Zhang et al., 2023). Thus, in this paper, Jeong's method was applied to correct the blockage effects in the wind tunnel experiment.

4.3 Effect of Wind Speed and Geometric Parameters

To consider the coupling effects among various geometric parameters, this study adopts a full-factor experimental design. The independent variables include the number of blades n, oscillation of deflector blade β_{out}, blade arc length s, installation angle of blade frame δ, and wind speed V_∞. Figure 9 shows the effects of these geometric parameters on the performance of the turbine. The maximum power coefficient ($C_{p,max}$) indicates the maximum efficiency obtained by the wind turbine at all *TSR*s. The results show that the flexible oscillating wind turbine can achieve a high $C_{p,max}$ at relatively low wind speeds. Under various geometric parameters, the $C_{p,max}$ of the wind turbine slightly increases with the increase of wind speed. The number of blades n, oscillation of deflector blade β_{out}, blade arc length s, installation angle of blade frame δ_{out} have a significant interaction effect on the $C_{p,max}$ of the wind turbine. The optimal geometric parameters are n =6 and β_{out} = 35°, s = 745 mm, δ = −15°, at which $C_{p,max}$ of the wind turbine is around 20%. When the installation angle of the blade frame δ is set at 15°, or when the blade arc length s is set at 740mm, the $C_{p,max}$ of the wind turbine tends to be relatively small. This phenomenon occurs because these specific configurations yield a smaller orientation angle α in the inflow region, which subsequently impedes the incoming flow from entering the turbine cavity. When the oscillation of deflector blade β_{out} is

35°, the $C_{p,max}$ of the wind turbine is the highest. At this configuration, the incoming flow is guided by the deflector blades, reducing the incoming flow speed in the upstream region, and changing the inflow direction so that the blades in the inflow region can present a large angle of attack with the inflow. However, when the oscillation of deflector blade β_{out} is 25°, deflector blades form a large angle of attack with the inflow, reducing the inflow speed. When the oscillation of deflector blade is 45°, the inflow cannot be effectively guided by the deflector blades.

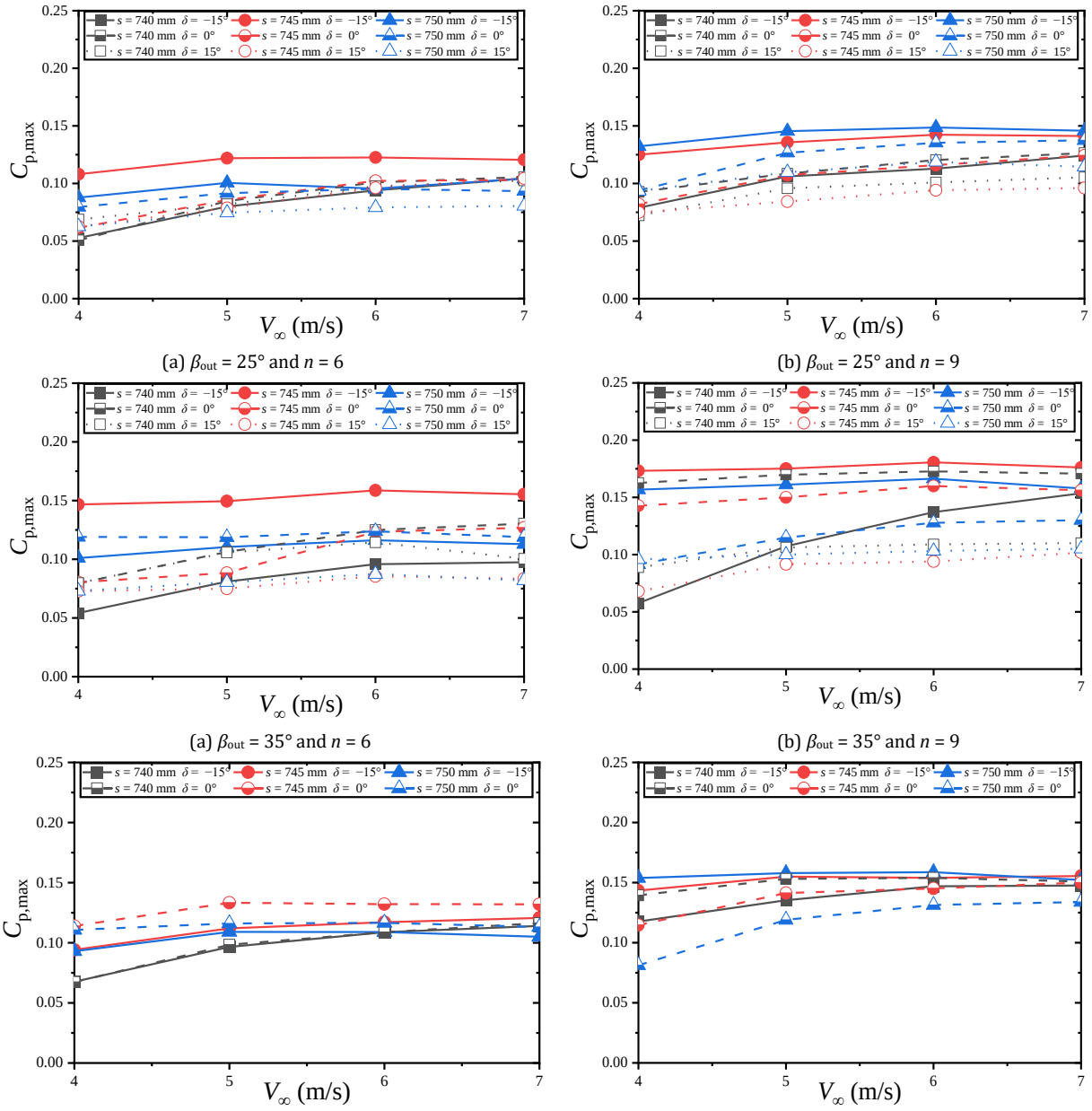

(a) β_{out} = 25° and n = 6 (b) β_{out} = 25° and n = 9

(a) β_{out} = 35° and n = 6 (b) β_{out} = 35° and n = 9

(a) β_{out} = 45° and n = 6 (b) β_{out} = 45° and n = 9

Figure 9: Variation in $C_{p,max}$ with wind speed and geometric parameters

5. Conclusion

This paper proposes a novel flexible oscillating wind turbine that achieves high efficiency by altering the pitch angle at different, eliminating the need for supplementary mechanical devices. To unravel the internal flow field mechanism of this wind turbine, Particle Image Velocimetry (PIV) experiments were conducted using the principle of similarity. Moreover, a wind tunnel-based parametric study was conducted to explore the impact of critical geometric parameters and wind speed on the turbine's performance. The key discoveries of this paper can be summarized as follows:

1. PIV experiments allowed the documentation of the time-varying orientation angle α of turbines under various azimuth angles θ. Notably, in the azimuthal range of 270° to 90°, the turbine's orientation angle α closely approaches the optimal value, thus generating considerable positive torque. In the downstream region (with an azimuth angle between 225° and 315°), blades stay in a diversion state, maintaining a minor angle of attack to avoid the generation of excessive negative torque.

2. Results of wind tunnel experiment reveal significant interactive effects on the maximum power coefficient $C_{p,max}$ of the wind turbine from the number of blades n, oscillation of deflector blade β_{out}, blade arc length s, and blade frame installation angle δ_{out}. Specifically, when the blade forms a large angle of attack in the inflow region, a noticeable decrease in the turbine's $C_{p,max}$ is observed.

3. The flexible oscillating wind turbine shows high efficiency even at lower wind speeds. The wind turbine can reach a $C_{p,max}$ of nearly 0.2 even when the wind speed is as low as 4m/s.

References

Akwa, J.V., Vielmo, H.A., Petry, A.P., 2012. A review on the performance of Savonius wind turbines. Renewable and Sustainable Energy Reviews, 16, Pp. 3054–3064.

Douak, M., Aouachria, Z., Rabehi, R., Allam, N., 2018. Wind energy systems: Analysis of the self-starting physics of vertical axis wind turbine. Renewable and Sustainable Energy Reviews 81, Pp. 1602–1610.

ElCheikh, A., Elkhoury, M., Kiwata, T., Kono, T., 2018. Transient analysis of H-type Vertical Axis Wind Turbines using CFD. Journal of Wind Engineering and Industrial Aerodynamics, 180, Pp. 19–33.

Elkhoury, M., Kiwata, T., Aoun, E., 2015. Experimental and numerical investigation of a three-dimensional vertical-axis wind turbine with variable-pitch. Journal of Wind Engineering and Industrial Aerodynamics 139, Pp. 111–123.

Fang, Z., Tan, J., Ji, G., Yuan, P., Sun, Z., Wang, S., 2022. Tehnical development status and prospect of flexible sails of unmanned sailboats. Chinese Journal of Ship Research 17, Pp. 183–193.

Glauert, H., 1935. Airplane Propellers, in: Aerodynamic Theory: A General Review of Progress Under a Grant of the Guggenheim Fund for the Promotion of Aeronautics. Springer Berlin Heidelberg, Berlin, Heidelberg, Pp. 169–360.

Guo, Y., Li, X., Sun, L., Gao, Y., Gao, Z., Chen, L., 2019. Aerodynamic analysis of a step adjustment method for blade pitch of a VAWT. Journal of Wind Engineering and Industrial Aerodynamics, 188, Pp. 90–101.

GWEC, 2022. Global Wind Report 2022. Global Wind Energy Council.

Islam, M.R., Mekhilef, S., Saidur, R., 2013. Progress and recent trends of wind energy technology. Renewable and Sustainable Energy Reviews 21, Pp. 456–468.

Jeong, H., Lee, S., Kwon, S.D., 2018. Blockage corrections for wind tunnel tests conducted on a Darrieus wind turbine. Journal of Wind Engineering and Industrial Aerodynamics, 179, Pp. 229–239.

Jiang, H., Cao, S., Cheng, Z., 2011. Advances in flexible sensors with MXene materials. Chinese Journal of Applied Mechanics, 28, Pp. 518–520.

Kinsey, T., Dumas, G., 2017. Impact of Channel Blockage on the Performance of Axial and Cross-Flow Hydrokinetic Turbines. Renewable Energy, 103, Pp. 239–254.

Maskell, E.C., 1963. A theory of the blockage effects on bluff bodies and stalled Wings in a closed wind tunnel.

Miliket, T.A., Ageze, M.B., Tigabu, M.T., 2022. International Journal of Green Energy, Pp. 1–38.

Rezaeiha, A., Kalkman, I., Blocken, B., 2017. Effect of pitch angle on power performance and aerodynamics of a vertical axis wind turbine. Applied Energy, 197, Pp. 132–150.

Ross, H., Polagye, B., 2020. An experimental assessment of analytical blockage corrections for turbines. Renewable Energy, 152, Pp. 1328–1341.

Sahu, B.K., 2018. Wind energy developments and policies in China: A short review. Renewable and Sustainable Energy Reviews, 81, Pp. 1393–1405.

Tian, W.L., Song, B.W., Mao, Z.Y., 2014. Wind Engineering, 38, Pp. 109–116.

Tummala, A., Velamati, R.K., Sinha, D.K., Indraja, V., Krishna, V.H., 2016. A review on small scale wind turbines. Renewable and Sustainable Energy Reviews, 56, Pp. 1351–1371.

Zhang, D., Guo, P., Cheng, Y., Hu, Q., Li, J., 2023. Analysis of blockage correction methods for high-solidity hydrokinetic turbines: Experimental and numerical investigations. Ocean Engineering 283, Pp. 115185.